applied sciences

MDPI

Article

Assessment of Modal Characteristics of Steel–Concrete Composite Girder Bridge with V-Shaped Piers

Yong Zeng [1,2,*], Xuan He [1,2], Yongqi Li [1,2] and Jianting Zhou [1,2]

[1] State Key Laboratory of Mountain Bridge and Tunnel Engineering, Chongqing Jiaotong University, Chongqing 400074, China
[2] Engineering Research Center of Ministry of Education for Mountain Bridge Structures and Materials, Chongqing Jiaotong University, Chongqing 400041, China
* Correspondence: yongzeng@cqjtu.edu.cn; Tel.: +86-13883238757

Abstract: As the standards of bridge design and construction continue to improve, more and more combination bridges are being put into use. The public's demand for aesthetically pleasing bridges is also increasing, making it necessary to use the special structure of steel–concrete combinations, continuous V-shaped piers, and continuously stiffened bridges. This structure has the structural and mechanical characteristics of both a continuous girder and a V-shaped pier bridge. The span can be reduced to a certain extent because the support of the V-shaped piers can be applied directly to the main girder. The spanning capacity of the bridge is generally greater than that of a combined steel–concrete girder bridge with vertical piers. The whole bridge is continuous, without expansion joints, making it more stable and safe for traffic. At present, research on this structural bridge type is not yet complete. In this paper, the structural system and dynamic characteristics of this bridge are investigated in the context of real-life engineering. Firstly, the self-vibration characteristics of the three structures were analyzed, and their effects on the self-vibration characteristics were studied by varying the height of the crossbeam at the V-shaped piers' support, the main beam stiffness, and the V-shaped piers' stiffness in the three structures. The results show that the increase in main beam stiffness can effectively improve the vertical stiffness of the three structures, with the most obvious effect on structure one and the least effect on structure two; the increase in V-shaped pier stiffness causes a huge improvement in the transverse stiffness of the three structures. Subsequently, a two-unit rod system model of the background bridge was established using the finite element method, and the original model was improved by calculating the equivalent shear stiffness of the shear nail group so that it could simulate the shear joints more accurately. The effects of the shear connectors on the self-vibration characteristics of the steel–concrete combined continuous beam–V-shaped piers and continuous rigid-frame bridge were investigated through theoretical analysis and finite element simulation. It was found that due to the existence of flexible shear connectors, the interface between the steel beam and concrete slab in the combined beam has a slippage effect which causes the deformation to become unsynchronized, and there is a certain difference between vibration patterns. The stiffness of the shear connectors has a certain effect on the self-vibration frequency of the bridge. The damage to the local shear connectors does not have a large effect on the self-vibration frequency of the overall structure, but the damage to the shear connectors at the beginning of the connection between the V-shaped piers and the main beam is greater than that of the other areas. Damage to shear joints should be given special consideration in comparison to other areas.

Keywords: steel–concrete composite girders; V-shaped pier bridges; shear connectors; two-unit rod system model

check for updates

Citation: Zeng, Y.; He, X.; Li, Y.; Zhou, J. Assessment of Modal Characteristics of Steel–Concrete Composite Girder Bridge with V-Shaped Piers. *Appl. Sci.* **2023**, *13*, 3421. https://doi.org/10.3390/app13063421

Academic Editor: Giuseppe Lacidogna

Received: 6 January 2023
Revised: 1 March 2023
Accepted: 2 March 2023
Published: 8 March 2023

Copyright: © 2023 by the authors. Licensee MDPI, Basel, Switzerland. This article is an open access article distributed under the terms and conditions of the Creative Commons Attribution (CC BY) license (https://creativecommons.org/licenses/by/4.0/).

1. Introduction

With the improvements in bridge construction, the level of infrastructure construction has also made great progress. A variety of beautiful and unique bridge structures have been

created. The aesthetic requirements of the public with regard to bridges have prompted the use of the special structure of a steel–concrete composite continuous beam with V-shaped piers on a continuous rigid bridge.

The superstructure of the bridge adopts a steel–concrete composite structure in which the reinforced concrete slab is under pressure at the top and the steel beam is under tension at the bottom, making full use of the material properties. At the same time, this structure can be constructed quickly, has a low building height, is light, has good structural ductility, can be built in the city without erecting supports, and generates less noise during construction; it not only meets the design specifications, but also has the advantages of both steel and concrete bridges. These benefits fully meet the current social development requirements for building environmental protection [1]. Reinforced concrete structures, on the other hand, continue to predominate in small and medium-span bridges. Research on the adoption of steel bridges for small and medium spans has received a positive response and has important practical significance.

The bridge substructure in this paper is a composite of vertical piers and V-shaped piers, with supports at the vertical piers and bolts between the V-shaped piers and the main girder thus forming a unique continuous beam–V-shaped pier continuous rigid structure. It makes the superstructure look slimmer, thus making the shape more beautiful [2].

Steel–concrete composite bridges appeared as early as the last century. In early composite structures, no shear connectors existed, and the concrete slabs were connected to the steel beams mainly by friction and bonding [3]. This design made the steel–concrete composite interface susceptible to slip effects, resulting in damage to the overall structure [4]. Since the 1930s, more and more research has been conducted on steel–concrete composite structures, and many bridges with steel–concrete composite structures have been built in Europe, the United States, and other developed countries. Steel–concrete bridges were rapidly developed in the 1960s, and not only did plasticity theory emerge as the theoretical foundation, but research methods also advanced to the nonlinear spatial level. From small- and medium-span bridges to large-span cable-stayed bridges, steel–concrete composite structures developed significantly in the 1990s [5]. The spacing of traditional steel main girders was increased in France, and the Hopital Bridge was built with only two steel main girders. The structure was easy to build, allowing its material properties to be fully utilized and greatly reducing construction and maintenance costs. This bridge has since become a model for the use of combined steel and concrete structures in the design and construction of short- and medium-span bridges.

Many experts and scholars have conducted studies on the slip action of steel–concrete composite structures, and many constructive conclusions have been reached. Several equations are proposed to determine the critical point at which a compressed bottom flange may buckle laterally in an unstable manner, i.e., lateral torsional buckling (Fragoso Dias, Joo Victor et al. [6]). Closed-form solutions for stress, deflection, and slip of box beams under lateral loading were obtained, and the comparison of the analytical results and the experimental results for steel–concrete composite box beams under concentrated loading or uniform loading verified the closed-form solution (Wang-bao Zhou et al. [7]). This emphasized the relative significance of the partial shear interaction within the full interaction, which has been addressed with the help of a parametric study considering various influencing parameters such as the degree of shear connection, span length, type of loading, distribution of shear stud connectors, geometry of the steel girder, yield strength of structural steel, and concrete grade (Madhusudan G. Kalibhat et al. [8]). Straight composite steel–concrete beams were tested to investigate their mechanical performance under combined negative bending and torsional moments (Lin Weiwei [9]). According to the experimental data of the steel beams of the Honglu Steel Company, a continuous composite and newer finite element model are presented (Liang Li Xiao et al. [10]). The model takes into account the effect of linear material, the slip between concrete and steel beams, and pre-stress. Five samples of a steel–concrete composite beam are calculated with the model, and the stress, strain, and crack propagation of the nonlinear numerical simulation analysis

are carried out; then, the continuous composite cross in the load deflection curve of beams is obtained. Based on the model test, the structural fatigue analysis of the OSD is carried out using the extended finite element method (XFEM) to understand and reveal the causes of fatigue detail cracks and the generation and propagation of fatigue cracks at the welding ends of diaphragms and U-ribs, which are the main structural fatigue details of the deck. The cutouts of diaphragms and the weld tips of the U-rib–diaphragm connections are very complex structural details in orthotropic steel decks, and are accordingly highly vulnerable to fatigue cracking. The majority of fatigue cracks in these details appear as a result of stress concentrations and initial weld defects. To determine the reason for the high probability of occurrence of fatigue cracks in these types of fatigue detail categories, a numerical model was established, using the extended finite element method (XFEM) to analyze the cracking of the diaphragm of an experimental 1:2-scaled deck segment model (Zeng, Yong et al. [11,12]). In order to study the feasibility and the working mechanism of improving the crack resistance of continuous steel–concrete composite bridges by releasing the interfacial slip effect within the negative bending moment region, two groups of model tests were carried out. This study is helpful for understanding the relationship between the interface slip and anti-crack characteristics in negative moment zones, and a new anti-crack design method is proposed for the design of continuous composite girders (Wu Wenqing et al. [13] A linear stiffness reduction method is proposed for calculating the stiffness of steel–concrete composite beams in the negative moment region after the concrete undergoes cracking. The proposed method can be used in engineering applications as it enables the facile and accurate calculation of the deflection and slip and the changes in stiffness of steel–concrete composite beams in the negative moment region (Cao W. et al. [14]). A theoretical model to describe shear-slip in steel–concrete–steel composite structures with bidirectional thin-walled webs is proposed chiefly by introducing a slip reduction factor (Guo, Y. et al. [15]). Based on the energy principle, a calculation method of the interfacial bond stiffness of steel–concrete composite beams was proposed, and the interfacial bond-slip constitutive relation of steel–concrete composite beams was given (Dong, S. et al. [16]). An improved theoretical interfacial stress and slip analysis is presented for a simply supported composite steel–concrete beam bonded with an adhesive (Dong, S. et al. [17]).

The existing studies mainly focus on the interface slip effect of general steel–concrete composite girders, and few scholars have studied the effect of shear connectors on the overall structural self-vibration characteristics of bridges; the study of shear connectors in steel–concrete composite continuous girder V-shaped pier continuous rigid-frame bridges is even more rare [18,19].

2. Bridge Description

The paper investigates a steel–concrete composite continuous girder V-shaped pier continuous rigid-structure bridge. The span arrangement of the bridge is 20 m + 24 m + 34 m + 56 m + 34 m. The superstructure is a steel–concrete structure consisting of two I-beam main girders and a concrete deck slab, and the cross girders are only connected to the steel main girders and not in contact with the concrete deck slab. The upper structure is continuous, with expansion joints only at the bridge abutment. The lower structure is a composite of vertical piers and V-shaped piers, of which P1 and P2 piers are vertical piers with bearings; P3 and P4 piers are V-shaped piers, and the main girders are fastened by high-strength bolts. The bridge elevation layout is shown in Figure 1.

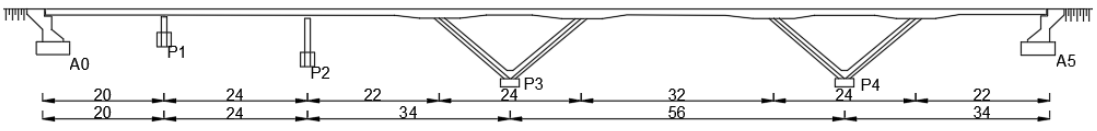


Figure 1. Elevation layout of the bridge/m.

A superstructure cross-sectional drawing of the bridge is shown in Figure 2. As shown in Figure 2, the concrete deck slab is made of a precast reinforced concrete structure, and each precast deck slab is 8.9 m long and 3 m wide. Four shear nail group holes are left on the precast slab, and the shear nail group is combined with the wet joint cast-in-place construction. The steel girder adopts the form of a variable section.

The deck slab is made of reinforced concrete with a thickness of about 0.3 m at the centerline and 0.35 m at the location at which it is combined with the pegs, and the single precast slab is a whole slab in the cross-bridge direction with four shear nail group holes reserved. The precast slab is 8.9 m long in the transverse direction and 3 m wide in the longitudinal direction, and each precast slab is connected by welding the reinforcement of the transverse wet joints as a whole and forming a combined system with the steel main beam through the shear nail group. The height of the steel main girders is 2.32 m at the top of the V-shaped piers and 1.52 m at the middle of the span, and the steel structure of the bridge is made of Q345 weathering steel, which has strong corrosion resistance and is lighter and easier to construct than ordinary steel. See Figure 3 for background bridge elevation photo.

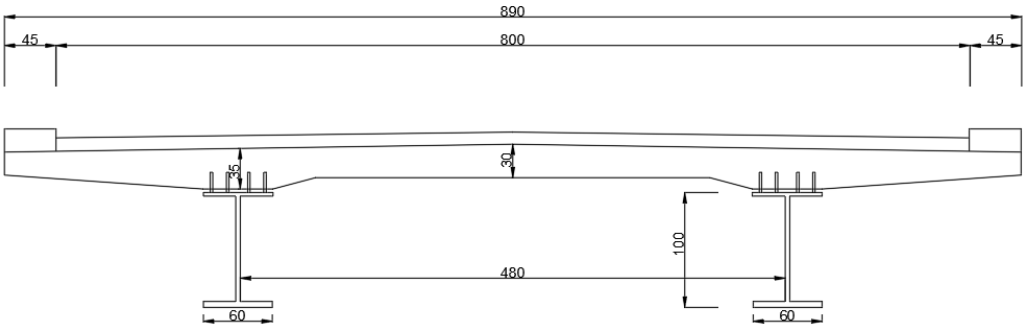


Figure 2. Typical bridge cross-section/cm.



Figure 3. Elevation of the whole bridge.

3. Finite Element Modeling

The finite element software Midas Civil was used to establish the whole bridge rod system unit model. There are 630 nodes and 584 units in total, and the model of the whole bridge is shown in Figure 4. The modeling parameters are shown in Tables 1 and 2.

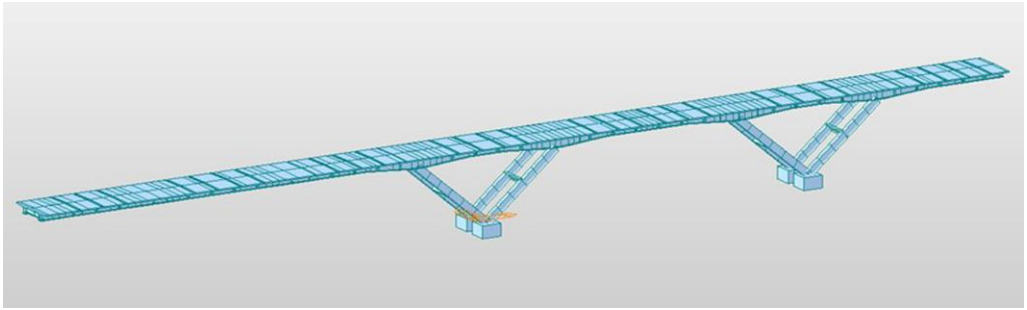


Figure 4. Full bridge model diagram.

Table 1. Bridge deck modeling parameters.

Concrete Grade	Modulus of Elasticity (MPa)	Poisson's Ratio	Standard Value of Axial Compressive Strength/Design Value (MPa)	Axial Tensile Strength Standard Value/Design Value (MPa)	Coefficient of Thermal Expansion
C40	32,500	0.2	26.8/19.1	2.39/1.71	0.00001

Table 2. Steel main beam and V-shaped pier modeling parameters.

Material Type	Q345D
Tensile strength	470–630
Yield stress	345(t $\leq$ 16 mm) 325(t > 16~35 mm)
Allowable shear stress under design load	120
Allowable shear stress under ultimate load	199.2(t $\leq$ 16 mm) 187.6(t > 16~35 mm)

The cross sections of the concrete slab and steel main beam are established separately by using the two-element modeling method. In the element division, the concrete deck slab and the steel main beam are divided into sections of the same length and number in the longitudinal direction, and then the concrete deck slab units are connected with the i and j ends of the steel main beam units at the same position to form a whole. The cross-sectional diagram of the concrete deck slab and steel girder of the two-unit model is shown in Figure 5.

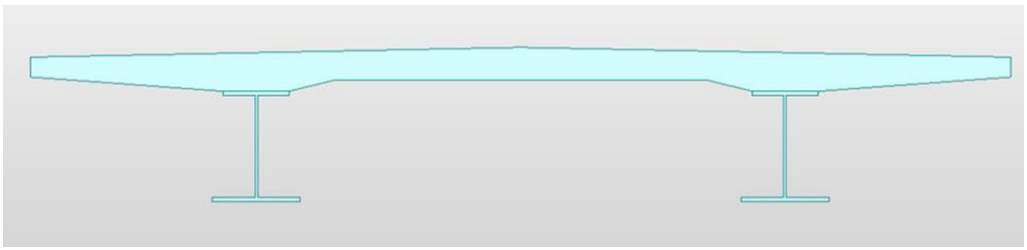
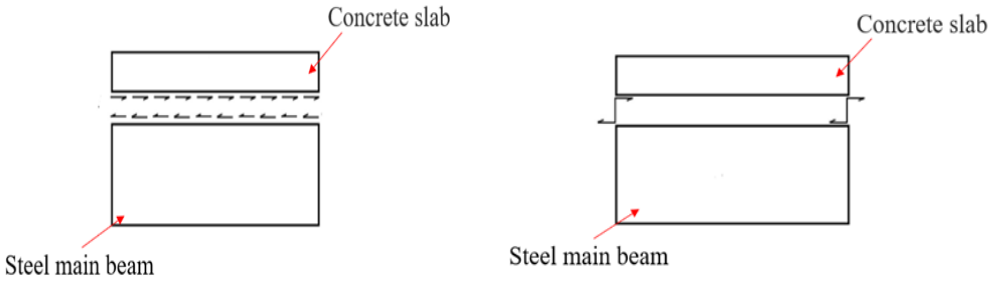


Figure 5. Cross-section of the two-element model.

This model differs from the combined section model in that the shear forces are not uniformly transferred between the steel–concrete composite interface, and the concrete deck slab and the steel main beam deform in concert only at the two ends of the unit. In contrast, the shear forces are uniformly distributed between the concrete deck slab unit and the steel girder unit in the combined section model. The schematic diagrams of the two types of cross-sections are shown in Figure 6.



(**a**) (**b**)

Figure 6. (**a**) Schematic diagram of combined section force transmission; (**b**) schematic diagram of double unit section force transmission.

Due to the different methods of force transmission, the two-unit model will have certain errors; however, when the model is fine enough to use the two-unit section to build the rod system model, it has a higher accuracy, while the calculation of the simulation is relatively simple.

4. Finite Element Model Optimization

The two-unit rod system model established by the conventional method cannot accurately simulate the shear joint action because the concrete deck slab and the steel main beam units are directly solidified, and the solid model would make the calculation too complicated. Here, the equivalent shear stiffness is used to optimize the finite element model to simulate the action of the shear connectors.

The stiffness parameter of a single shear nail can be calculated from Equation (1) according to the code [20] for welded nail connectors:

$$k_{ss} = 13.0 d_{ss} \sqrt{E_c f_{ck}} \quad (1)$$

Among them:

k_{ss} indicates the shear stiffness of the peg (N/mm);
d_{ss} indicates the diameter of the peg (mm);
E_c indicates the concrete elastic modulus (MPa);
f_{ck} indicates the standard value of compressive strength of concrete (MPa).

The vertical stiffness of the shear nail can be viewed as a whole as an axially tensioned bar; its vertical deformation can be regarded as a vertical lift-off displacement. The stress is proportional to the strain when it is in the elastic phase, and the calculation formula is shown in Equation (2), which can simplify its vertical stiffness to 10 times the lateral stiffness [21].

$$k_v = \frac{E_{st} A_{st}}{l} \quad (2)$$

Among them:

k_v indicates the vertical stiffness of the peg (N/mm);
E_{st} indicates the modulus of elasticity of the peg (MPa);
A_{st} indicates the cross-sectional area of the spigot bar (mm^2);
l indicates the length of the spigot rod (mm).

For the equivalent shear bearing capacity of the shear nail group, the formula for the equivalent stiffness of the shear nail group is proposed by calculating the strain energy generated by the deformation of the shear nail and concrete [22]. When the shear nail group is in the elastic deformation, the calculation formula is

$$K = n\beta \cdot \frac{(b-d)^2}{h} G_c \quad (3)$$

Among them;

n indicates the number of transverse rows of the shear nail group;
β is a constant related to the material properties of the shear nail;
b indicates the total directional spacing along the shear transfer release direction;
d indicates the diameter of the shear nail (mm);
h denotes the height of the shear nail (mm);
G_c indicates the shear modulus of concrete (MPa).

From Equation (3), it can be seen that the equivalent stiffness of the shear nail group when the shear nail is in the elastic phase is only related to the shear nail arrangement form, the shear nail structure form, and the concrete shear modulus of elasticity.

When the shear nail enters the plastic state, the equivalent shear stiffness of the shear nail group is

$$\mathrm{K} = \mathrm{n}\frac{\pi d}{4}G_p \tag{4}$$

where G_p denotes the hardening modulus of the steel after it enters the plastic state (MPa).

The shear connectors are simulated by the equivalent stiffness of the shear nail group and the calculated equivalent stiffness to elastically connect the concrete deck slab units to the steel girder units.

5. Analysis of Structural Self-Vibration Characteristics

For the analysis of the special structure of the steel–concrete combined continuous beam–V-shaped pier continuous rigid structure, the following two structures were assumed by changing the setting of the bearings on the basis of the original structure.

Structure I: The bearing is set at the bottom of the V-shaped piers, and the overall structure is a continuous girder bridge with V-shaped supports.

Structure 2: The original vertical pier bearings are removed and the vertical pier is cemented to the main girder, so the overall structure is a continuous rigid bridge with V-shaped supports.

The subspace iterative method is often used when performing large-scale finite element calculations. It is a highly efficient method for calculating the dynamic response of a structure, requiring only the calculation of low-order eigenvalues and corresponding eigenvectors. In this section, the subspace iterative method is used to analyze the self-oscillation characteristics of the structure [23,24].

5.1. Influence of the Height of the Crossbeam at the Connection between the V-Shaped Piers and the Main Beam on the Self-Vibration Characteristics

The height of the main girder at the connection between the V-shaped piers and the main girder has been increased, and the stiffness of the crossbeam here has a significant impact on the overall stiffness of the bridge. The original beam height of 1.064 m is now adjusted in increments of −0.2, −0.1, 0, 0.1 and 0.2 m, respectively, with the effect of the change in beam height at the connection between the V-shaped piers and the main beam on the modal self-vibration frequencies of each order shown in Table 3 and Figure 7.

The results of the calculations show that the first tenth-order vibration patterns of the three structures do not change after changing the height of the beam at the V-shaped piers, indicating that the effect of the height of the beam at the V-shaped piers is small. The first-order vertical vibration of all three structures is negatively correlated with the height of the crossbeam at the V-shaped piers and positively correlated with the first-order vertical vibration before the first-order vertical vibration occurs. This indicates that the crossbeam at the V-shaped piers not only increases the lateral stiffness of the bridge, but also has an effect on the structural stiffness of the V-shaped piers, with the most significant effect on Structure 2.

Table 3. Self-vibration frequencies (Hz) for different beam heights of the original structure.

Modal Order	Self-Vibration Frequency				
	−0.2	**−0.1**	**0**	**0.1**	**0.2**
1	1.40	1.40	1.40	1.41	1.41
2	1.91	1.91	1.91	1.91	1.91
3	3.73	3.73	3.73	3.73	3.73
4	3.95	3.95	3.95	3.95	3.94
5	4.36	4.37	4.37	4.37	4.37
6	4.79	4.79	4.79	4.79	4.79
7	5.28	5.28	5.28	5.28	5.28
8	6.18	6.18	6.18	6.18	6.18
9	6.66	6.66	6.66	6.66	6.66
10	7.68	7.68	7.68	7.68	7.68

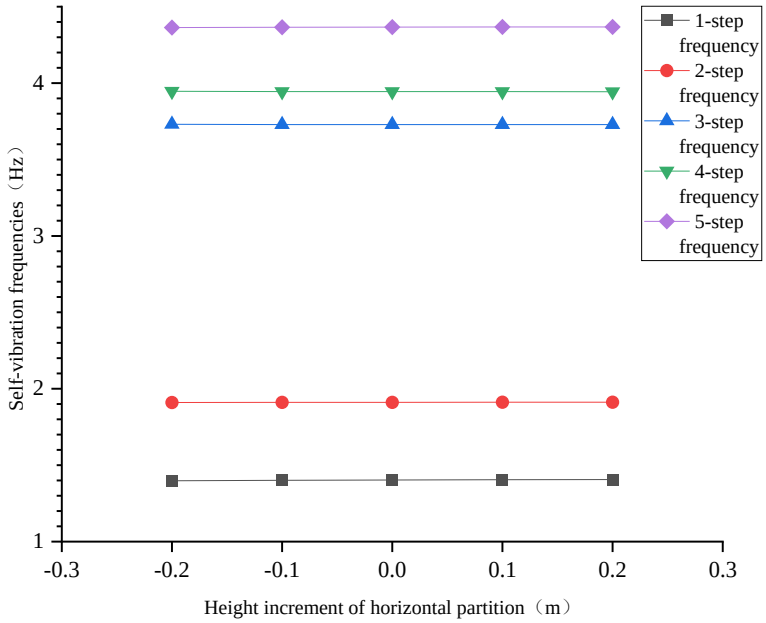


Figure 7. Self-vibration frequencies of the original structure at different beam heights.

All three structures have a small effect on the overall stiffness of the structure by changing the height of the crossbeam but still reflect a certain pattern. The first-order torsion frequency increases with the height of the crossbeam. It can be seen that the first-order torsion of all three structures occurs at the girder section at which the V-shaped piers are located.

5.2. Influence of Main Beam Stiffness on Self- Vibration Characteristics

As the frequency of structural self-vibration is positively related to the stiffness of the structure, both the girder and V-shaped piers are the main load-bearing members of the structure, and changes in the stiffness of the girder and V-shaped piers have a great influence on the self-vibration characteristics of the structure. By maintaining the beam cross-section and changing its stiffness by varying the modulus of elasticity of the material, the structural self-vibration frequency and the variation of vibration pattern are analyzed.

The main beam flexural stiffness is varied by −10%, −5%, 5% and 10%, respectively, to analyze the changes in the self-vibration frequencies and vibration modes of the structure. The effect of the change in the main beam flexural stiffness on the self-vibration frequencies and vibration characteristics of each modal is shown in Tables 4–6 and Figures 8–10.

Table 4. Self-vibration frequencies (Hz) for different main beam stiffnesses of the original structure.

Modal Order	Self-Vibration Frequency				
	−10%	−5%	0	5%	10%
1	1.41	1.40	1.40	1.40	1.40
2	1.88	1.91	1.91	1.94	1.96
3	3.73	3.73	3.73	3.73	3.73
4	3.92	3.95	3.95	3.97	3.98
5	4.32	4.38	4.37	4.43	4.48
6	4.75	4.80	4.79	4.84	4.88
7	5.18	5.28	5.28	5.38	5.36
8	6.08	6.18	6.18	6.26	6.24
9	6.55	6.65	6.66	6.75	6.81
10	7.57	7.71	7.68	7.79	7.87

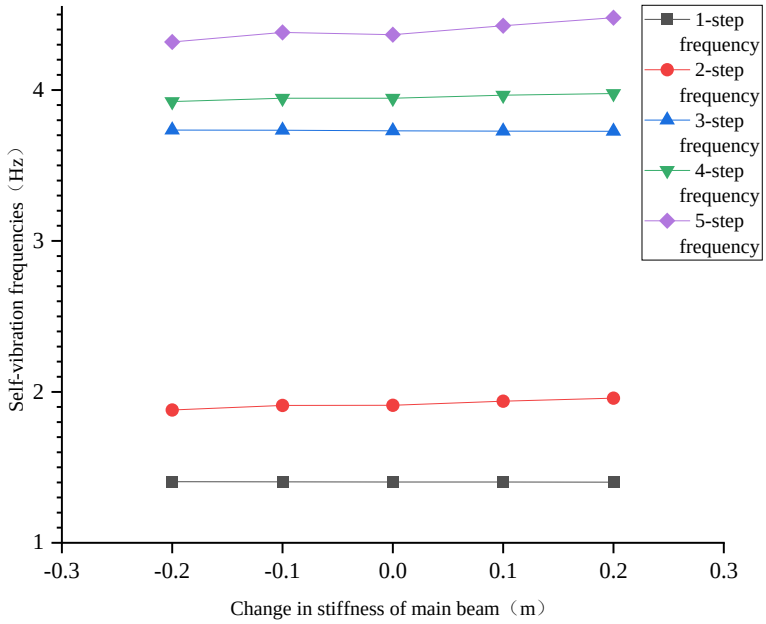


Figure 8. Self-vibration frequencies of the original structure for different main beam stiffnesses.

By analyzing the data, it can be seen that as the stiffness of the main beam increases, the fundamental frequency of the structure changes to a small extent, and the vibration pattern of each order remains unchanged. The first two orders of self-vibration frequencies are affected by the stiffness of the main beam to a small extent, and are mainly negatively correlated. The third-order self-vibration and the second-order vertical vibration frequency are affected by the stiffness of the main beam more significantly, and are positively correlated. The first-order vertical vibration frequency increases by 4.14% when the stiffness of the main beam is increased from −10% to 10%. The fifth-order self-vibration frequency decreases, but the sixth- to tenth-order self-vibration frequency increases to a greater extent, with the seventh-order self-vibration frequency increasing by 3.75%. This indicates that the increase in the stiffness of the main beam causes a significant increase in the vertical stiffness of the bridge, including the V-shaped piers, and has little effect on the transverse stiffness.

The effect of the stiffness changes of the main beam of Structure I is similar to that of the original structure, with the first-order vertical self-vibration frequency increasing by 5.59% when the stiffness of the main beam is increased from −10% to 10%. This indicates that the increase in the stiffness of the main beam has a greater effect on the vertical stiffness of Structure 1 compared to the original structure.

Table 5. Self-vibration frequencies (Hz) for different main beam stiffnesses of Structure I.

Modal Order	Self-Vibration Frequency				
	−10%	−5%	0	5%	10%
1	1.22	1.22	1.22	1.22	1.22
2	1.40	1.42	1.43	1.46	1.47
3	2.64	2.64	2.64	2.63	2.63
4	3.31	3.37	3.38	3.44	3.49
5	3.52	3.53	3.53	3.55	3.56
6	3.55	3.57	3.57	3.59	3.61
7	4.02	4.03	4.03	4.03	4.03
8	4.08	4.14	4.15	4.21	4.24
9	4.65	4.74	4.74	4.79	4.82
10	5.01	5.08	5.08	5.17	5.16

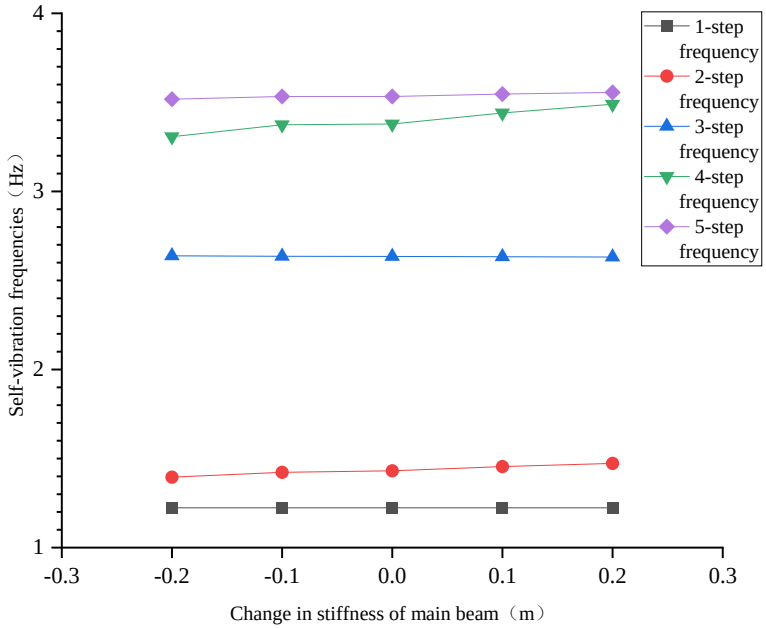


Figure 9. Self-vibration frequencies for different main beam stiffnesses of Structure I.

Table 6. Self-vibration frequencies (Hz) for different main beam stiffnesses of Structure II.

Modal Order	Self-Vibration Frequency				
	−10%	−5%	0	5%	10%
1	2.04	2.03	2.03	2.03	2.03
2	3.74	3.79	3.77	3.82	3.87
3	4.84	4.86	4.84	4.86	4.88
4	5.06	5.09	5.08	5.11	5.14
5	5.29	5.37	5.36	5.43	5.49
6	7.17	7.26	7.25	7.34	7.40
7	7.84	7.96	7.90	8.02	8.10
8	8.08	8.19	8.14	8.24	8.32
9	8.81	8.80	8.79	8.78	8.77
10	9.01	9.10	9.09	9.20	9.32

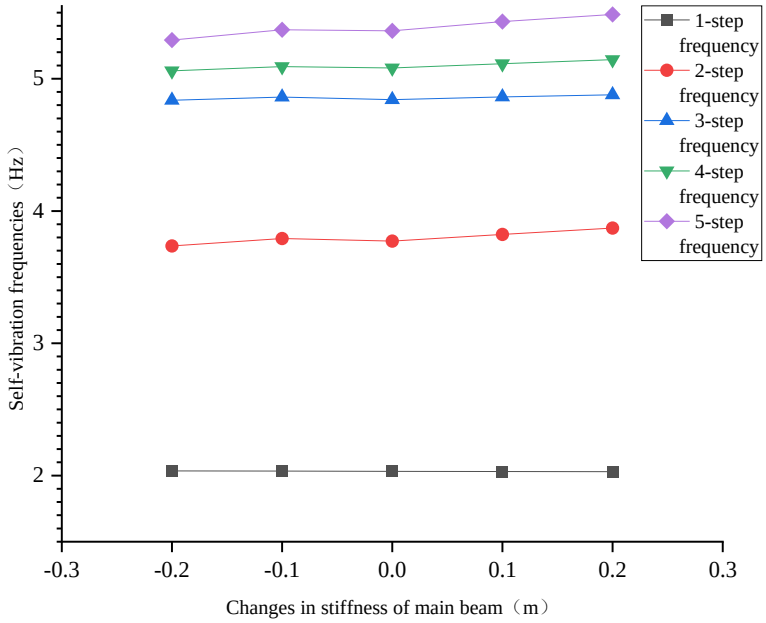


Figure 10. Self-vibration frequencies for different main beam stiffnesses of Structure II.

The first two orders of the self-vibration frequencies of Structure II decrease as the stiffness of the main beam increases, while the self-vibration frequencies from the third to ninth order increase with the stiffness of the main beam, but to a smaller extent.

5.3. Effect of V-Shaped Pier Stiffness on Self-Vibration Characteristics

The V-shaped piers' flexural stiffness was varied by −10%, −5%, 5% and 10% to analyze the changes in the self-vibration frequencies and vibration modes of the structure. The effects of the changes in the V-shaped piers' flexural stiffness on the self-vibration frequency and vibration characteristics of the modes are shown in Tables 7–9 and Figures 11–13.

The original structure has no change in the first ten orders of vibration after changing the V-shaped piers' stiffness, and the self-vibration frequencies increase to some extent with the increase in the V-shaped piers' stiffness. The first-order self-vibration frequency changes most significantly after the V-shaped piers' stiffness increases from −10% to 10%; increasing by 6.38%. The first-order vertical self-vibration frequency increased by 3%. The results show that increasing the V-shaped piers' stiffness can effectively increase the full bridge stiffness, as the full bridge transverse stiffness undergoes a large degree of improvement.

Table 7. Self-vibration frequencies (Hz) for different V-shaped pier stiffnesses of the original structure.

Modal Order	Self-Vibration Frequency				
	−10%	−5%	0	5%	10%
1	1.36	1.38	1.40	1.43	1.45
2	1.88	1.90	1.91	1.93	1.94
3	3.72	3.72	3.73	3.73	3.74
4	3.91	3.93	3.95	3.96	3.98
5	4.30	4.33	4.37	4.40	4.43
6	4.73	4.76	4.79	4.82	4.84
7	5.27	5.28	5.28	5.29	5.29
8	6.16	6.17	6.18	6.18	6.19
9	6.55	6.60	6.66	6.71	6.76
10	7.66	7.63	7.68	7.73	7.77

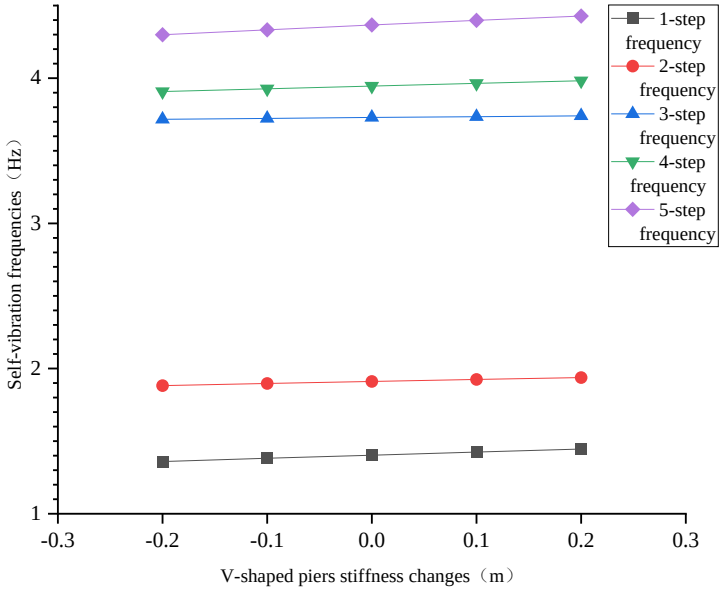


Figure 11. Self-vibration frequencies for different V-shaped pier stiffnesses of the original structure.

Table 8. Self-vibration frequencies (Hz) for different V-shaped pier stiffnesses of Structure I.

Modal Order	Self-Vibration Frequency				
	−10%	−5%	0	5%	10%
1	1.19	1.21	1.22	1.24	1.26
2	1.42	1.43	1.43	1.43	1.44
3	2.61	2.62	2.64	2.65	2.66
4	3.37	3.37	3.38	3.39	3.39
5	3.47	3.50	3.53	3.56	3.59
6	3.55	3.56	3.57	3.58	3.59
7	4.01	4.02	4.03	4.03	4.04
8	4.09	4.12	4.15	4.17	4.20
9	4.69	4.72	4.74	4.75	4.76
10	5.06	5.07	5.08	5.11	5.14

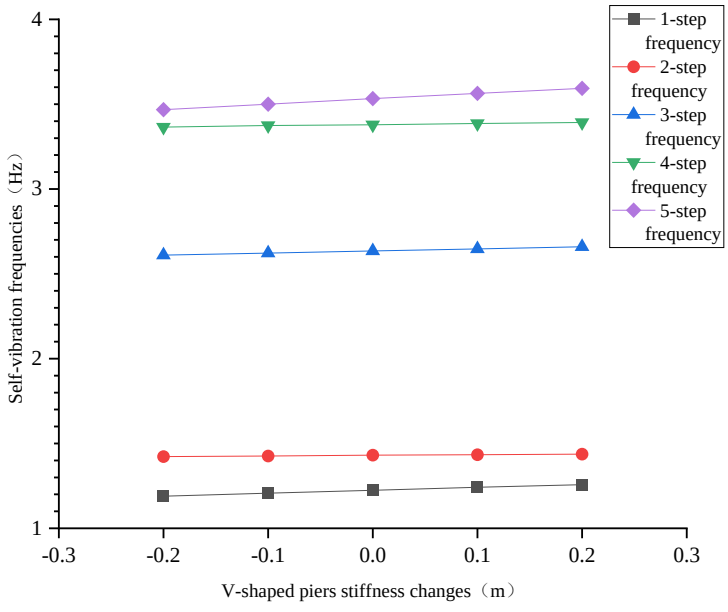


Figure 12. Self-vibration frequencies for different V-shaped pier stiffnesses of Structure I.

The pattern of variation in structure I with the V-shaped piers' stiffness is similar to that of the continuous beam–continuous rigid structure wherein the first-order self-vibration frequency increases by 5.734% as the V-shaped piers' stiffness varies from −10% to 10%.

Table 9. Self-vibration frequencies (Hz) for different V-shaped pier stiffnesses of Structure II.

Modal Order	Self-Vibration Frequency				
	−10%	−5%	0	5%	10%
1	1.99	2.01	2.03	2.05	2.07
2	3.72	3.74	3.77	3.80	3.82
3	4.80	4.82	4.84	4.86	4.88
4	5.05	5.07	5.08	5.10	5.11
5	5.27	5.32	5.36	5.41	5.45
6	7.13	7.19	7.25	7.32	7.37
7	7.78	7.84	7.90	7.96	8.02
8	8.00	8.07	8.14	8.20	8.26
9	8.78	8.78	8.79	8.80	8.81
10	8.93	9.02	9.09	9.16	9.22

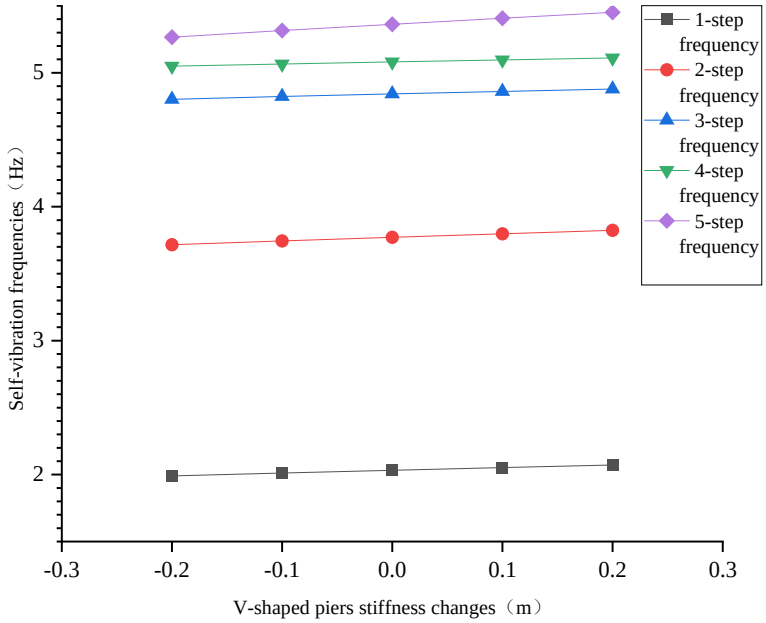


Figure 13. Self-vibration frequencies for different V-shaped pier stiffnesses of Structure II.

The first-order self-vibration frequency increases the most with increasing V-shaped pier stiffness, with the first-order self-vibration frequency of the continuous rigid structure increasing by 4.07% when the V-shaped piers' stiffness increases from −10% to 10%.

6. The Effects of Shear Connector on Self-Vibration Characteristics

6.1. The Effects of Shear Connector Stiffness

The concrete deck slab is set up in the finite element model with rigid connection (infinite stiffness), design stiffness elastic connection and one-half design stiffness elastic connection to the steel main beam, respectively. The first five orders of self-vibration frequencies are shown in Table 10. The first-order vertical formations of the rigid connection and the design stiffness elastic connection are shown in Figures 14 and 15.

Table 10. Effect of shear-resistant connectors on the self-vibration frequencies of the original structure.

Modal Order	One-Half Design Stiffness	Design Stiffness	Rigid Connection
1	1.396	1.403	1.410
2	1.882	1.911	1.939
3	3.678	3.729	3.777
4	3.924	3.945	3.967
5	4.283	4.366	4.446

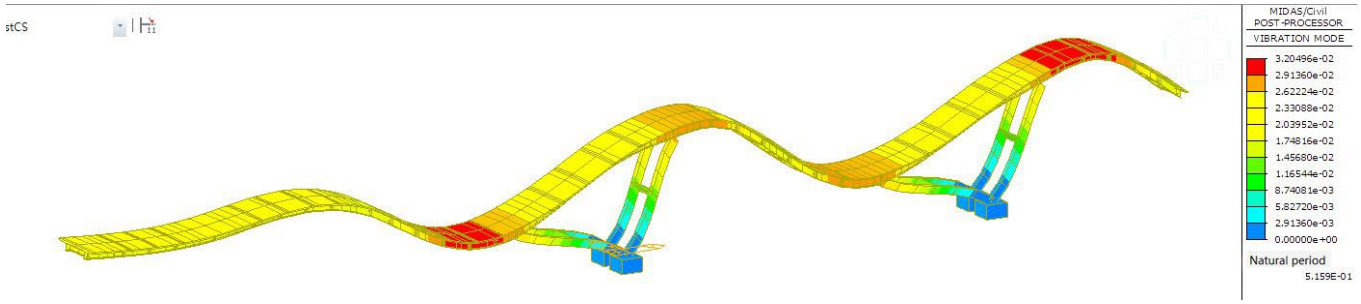


Figure 14. First-order vertical vibration diagram of rigid connection/m.

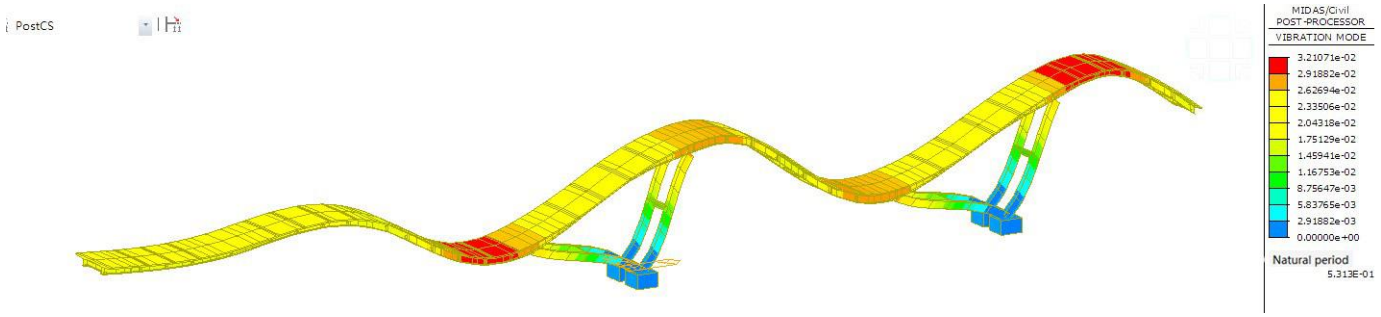


Figure 15. One-half design stiffness elastic connection first-order vertical vibration diagram/m.

It can be seen from Table 10 that if the slip effect between the deck plate and the steel main beam is not considered, i.e., if the deck plate is rigidly connected to the steel main beam, there will be a large increase in each order of the bridge's self-vibration frequency phase. The first-order vertical self-vibration frequency rises from 1.911 Hz to 1.936 Hz, with an increase of 1.5%. Due to the presence of flexible shear connectors, the interface between the steel beam and the concrete slab in the combined beam has slippage, causing the deformation of the two to become unsynchronized, and there is a certain phase difference between the vibration patterns. The first-order fundamental frequency of the structure has a great influence on the impact coefficient caused by the vehicle load, so the influence of the interface slip should be considered in the impact coefficient calculation of the bond beam.

6.2. Effect of Local Damage of Shear Joints

When the overall stiffness of the shear connectors decreases, the self-vibration frequency of the bridge decreases, but the loss of stiffness of the shear connectors is not uniform in the actual use of the bridge.

6.2.1. Shear-Resistant Connectors Vulnerable to Regional Damage

In the actual use process, the damage location of the shear connectors is difficult to determine; in the negative moment zone of the bridge, as the concrete deck slab is subjected to tensile stress compared with the positive moment zone of the compressive state, the concrete deck slab for the shear nail restraint effect is decreased. Therefore, in the

background bridge, the shear nail density is much higher than that of the span section at the connection between the bearing and the steel beam and V-shaped piers, which reduces the damage probability of the shear nails to some extent. Therefore, the shear connectors are considered to be damaged first in the mid-span area in which the deflection is the largest. The deflection diagram of the whole bridge is shown in Figure 16.

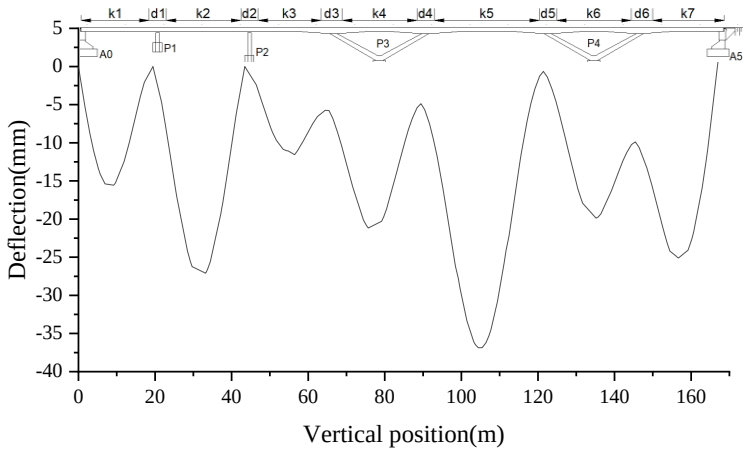


Figure 16. Schematic diagram of full bridge deflection.

From the above figure, it can be seen that the deflection value of the background bridge is higher in the second span, the fifth span and the seventh span mid-span area, and the damage of shear connectors is considered to occur preferentially in this third span mid-span area. In the second span (the fifth span and the seventh span), a shear joint damage zone with a length of 0.1 m was set up to simulate the local shear joint damage by changing the shear joint stiffness in this area. The shear joint damage zone is shown in Figure 17.

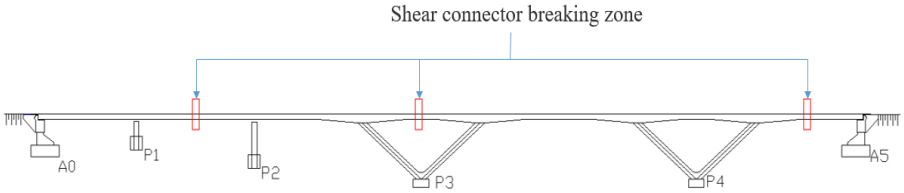


Figure 17. Schematic diagram of the damage zone of the shear resistant connector.

As the shear connectors are flexible connections in the form of shear nails, the form of damage incurred is generally ductile damage, so the damage zone shear connector stiffness were set to design stiffness, one half of the design stiffness, and stiffness to zero (complete damage); the self-vibration frequencies of the original bridge as shown in Table 11.

Table 11. Effect of damage to the vulnerable area of shear joints on the self-vibration frequency of the structure.

Modal Orders	Complete Destruction	Degree of Damage One-Half Design Stiffness	Design Stiffness
1	1.40	1.40	1.40
2	1.91	1.91	1.91
3	3.73	3.73	3.73
4	3.94	3.94	3.95
5	4.36	4.36	4.37

From the above table, it can be seen that the local damage of the shear connectors has little effect on the self-vibration frequencies of the bridge, especially the first two orders of self-vibration frequencies, which undergo almost no change; the third to fifth-order self-vibration frequency decreases with local damage to the shear connectors. This indicates that the local damage to the shear joint has almost no effect on the overall lateral stiffness of the bridge, but has a certain effect on the slight reduction of the vertical stiffness, and the vibration modes do not change with local damage to the shear joints. This may be due to the fact that after damage to the local shear joints, the shear joints in other areas still function, and the concrete deck slab and steel main girders are still in a synergistic state, which does not have a large impact on the overall structural self-vibration frequencies.

6.2.2. Effect of Damage to Shear Connectors on Self-Vibration Frequencies in Different Regions

It is known that different degrees of damage to shear joints in vulnerable areas will have some effect on the vertical stiffness of the overall structure. This section analyzes and compares the effect of damage to shear joints in different areas on the overall structural self-vibration frequencies [25,26].

Three areas of damage to shear connectors are set separately, assuming that the damage longitudinal bridge length is 0.1 m. The damage areas are as follows:

Area 1: P3# V-shaped piers and main beam connection near the A0# abutment side.

Area 2: 5th span across the middle region.

Area 3: V-shaped piers of Pier P4#, connected with the main beam near the side of the A0# abutment.

The damage area of the shear-resistant connector is shown in Figure 18.

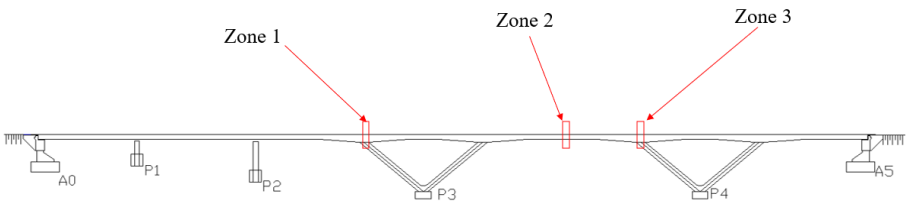


Figure 18. Different damage area settings for shear-resistant connectors.

The damage degree of the shear joints is set to complete damage, i.e., the case in which the shear stiffness is reduced to 0. The self-vibration frequencies of shear joints in different regions after damage are shown in Table 12.

Table 12. Effect of damage in different areas of shear joints on the self-vibration frequency of the structure.

Modal Orders	Area 1	Area 2	Area 3	No Damage
1	1.403	1.403	1.403	1.403
2	1.910	1.911	1.910	1.911
3	3.728	3.725	3.727	3.729
4	3.944	3.945	3.944	3.945
5	4.365	4.366	4.365	4.366

From the results in Table 12, it can be seen that because the selected areas are small, the effect on the overall structural self-vibration frequency is not significant, but still reflects a certain law. Area 1 and Area 3 are located in the connection area between the V-shaped piers and main beam, and the vertical stiffness of the structure is reduced when the shear joint is damaged, which shows that the shear joint has a greater influence on the overall vertical stiffness of the structure. When the damage occurred in Area 2, only the third-order self-vibration frequency, that is, the second-order vertical self-vibration frequency, was

reduced. The third-order vertical self-vibration mode of the bridge shows that the third-order self-vibration has the maximum amplitude in the fifth span. This demonstrates that only the third-order self-vibration frequency decreases when the shear joint is damaged in Area 2.

7. Conclusions

In this paper, a theory for calculating the equivalent stiffness of shear nail groups is introduced into a two-unit rod system model to optimize the model in order to accurately simulate the effect of shear connectors. In addition, considering the special characteristics of the steel–concrete combined continuous beam–V-shaped pier continuous rigid structure, two other structures are assumed by changing the settings of the bearings on the basis of the original structure, one of which is a continuous beam structure with V-shaped pier bearings at the base of the V-shaped piers. The other is a continuous rigid structure with V-shaped pier bearings with vertical piers and main beams. Using finite element analysis, the three structures are compared to analyze the characteristics and dynamic properties of the steel–concrete combined continuous beam–V-shaped pier continuous rigid structure. The effect of shear connectors on the self-vibration characteristics of the steel–concrete combined continuous girder-V-shaped pier continuous rigid-frame bridge is investigated. The results are as follows.

Analysis of the structural self-vibration characteristics shows that (1) the torsional stiffness of the beam section at the V-shaped pier support can be increased to some extent by increasing the stiffness of the top beam of the V-shaped piers; (2) the increase in the stiffness of the main beam can effectively improve the vertical stiffness of the three structures, with the most obvious effect on structure one and the least effect on structure two. The increase in the V-shaped piers' stiffness causes a huge improvement in the transverse stiffness of the three structures; and (3) the transverse stiffness of the three structures may be small, and the transverse stiffness of the different structures can be improved to a greater extent by increasing the V-shaped piers' stiffness.

The analysis of the effect of shear connectors on the self-vibration characteristics shows that (1) if the slippage of the bridge deck plate and steel main beam is not considered, i.e., if the bridge deck plate is rigidly connected to the steel main beam, there will be a large increase in the self-vibration frequency phase of each order of the bridge. Due to the existence of flexible shear joints, there is slippage at the interface between the steel beam and the concrete slab in the combined beam, causing the deformation to become unsynchronized, and there is a certain phase difference between the vibration patterns; (2) after the damage of the local shear joints, the shear joints in other areas still function, and the concrete deck slab and the steel main girders are still in a synergistic state, which will not have a large impact on the overall structural self-vibration frequencies; and (3) the damage to the shear connectors in the area in which the V-shaped piers are connected to the main beam has a greater effect on the overall structural self-vibration frequencies compared to that in other areas.

The proposed optimization measures for the two-unit rod system model have not been tested for shear nail rollout due to limited conditions, and the applicability of this model to simulate shear joints will be further verified. The structure of this type of bridge is very special, but the research on it is not yet complete, and we hope that the subsequent research on this structure can be furthered in order to popularize this attractive bridge structure.

Author Contributions: Writing—original draft, Y.L.; Writing—review & editing, X.H.; Supervision, Y.Z.; Funding acquisition, J.Z. All authors have read and agreed to the published version of the manuscript.

Funding: This research was funded by the Chongqing Returned Overseas Scholars' Entrepreneurship and Innovation Support Fund (cx2018113, cx2020117).

Institutional Review Board Statement: Not applicable.

Informed Consent Statement: Not applicable.

Data Availability Statement: All data generated or analyzed during this study are included in this article. All data included in this study are available upon request by contact with the corresponding author.

Acknowledgments: This paper was partially supported by the Natural Science Foundation of China (Grant No.51908093), the Chongqing Returned Overseas Scholars' Entrepreneurship and Innovation Support Fund (cx2018113, cx2020117), and the National Key Laboratory of Mountain Bridge and the Tunnel Engineering Development Fund (CQSLBF-Y14, CQSLBF-Y16-10).

Conflicts of Interest: The authors declare no conflict of interest regarding the publication of this paper.

References

1. Hadeed, R.S.; Issa, M.A. Impact of shear connectors on composite action in full-depth precast concrete bridge systems. *PCI J.* **2022**, *67*, 71–87. [CrossRef]
2. Llombart, J.A.; Revoltós, J.; Fernández, J. Teror Viaduct in Gran Canaria Island, Spain. *Struct. Eng. Int.* **2014**, *24*, 111–113. [CrossRef]
3. Wang, S.; Fang, Z.; Chen, G.; Jiang, H. Numerical Analysis on Shear Behavior of Grouped Head Stud Shear Connectors between Steel Girders and Precast Concrete Slabs with High-Strength Concrete-Filled Shear Pockets. *J. Bridge Eng.* **2021**, *26*, 6. [CrossRef]
4. Mackay, H.M.; Gillespie, P.; Leluau, C. Report on the strength of steel I-beams haunched with concrete. *Eng. J. Can.* **1923**, *6*, 365–369.
5. Costin, A.; Hu, H.; Medlock, R. Building Information Modeling for Bridges and Structures: Outcomes and Lessons Learned from the Steel Bridge Industry. *Transp. Res. Rec.* **2021**, *2675*, 576–586. [CrossRef]
6. Dias, J.V.F.; Oliveira, J.P.S.; Calenzani, A.F.G.; Fakury, R.H. Elastic Critical Moment of Lateral-Distortional Buckling of Steel-Concrete Composite Beams under Uniform Hogging Moment. *Int. J. Struct. Stab. Dyn.* **2019**, *19*, 1950079. [CrossRef]
7. Zhou, W.-B.; Jiang, L.-Z.; Liu, Z.-J.; Liu, X.-J. Closed-form solution for shear lag effects of steel-concrete composite box beams considering shear deformation and slip. *J. Central South Univ.* **2012**, *19*, 2976–2982. [CrossRef]
8. Kalibhat, M.G.; Upadhyay, A. Numerical study on the deformation behavior of steel concrete composite girders considering partial shear interaction. *Structures* **2019**, *23*, 437–446. [CrossRef]
9. Lin, W. Experimental investigation on composite beams under combined negative bending and torsional moments. *Adv. Struct. Eng.* **2020**, *24*, 1456–1465. [CrossRef]
10. Liang, L.; Ming, Y.; Jian, W. Nonlinear Finite Element Analysis of Continuous Steel-Concrete Composite Beams. *Appl. Mech. Mater.* **2014**, *638–640*, 159–162. [CrossRef]
11. Zeng, Y.; He, H.; Qu, Y.; Sun, X.; Tan, H.; Zhou, J. Numerical Simulation of Fatigue Cracking of Diaphragm Notch in Orthotropic Steel Deck Model. *Materials* **2023**, *16*, 467. [CrossRef]
12. Zeng, Y.; Qu, Y.; Tan, Y.; Jiang, Y.; Gu, A. Analysis of fatigue cracking of orthotropic steel decks using XFEM. *Eng. Fail. Anal.* **2022**, *140*, 106536. [CrossRef]
13. Wu, W.; Dai, J.; Chen, L.; Liu, D.; Zhou, X. Experiment Analysis on Crack Resistance in Negative Moment Zone of Steel–Concrete Composite Continuous Girder Improved by Interfacial Slip. *Materials* **2022**, *15*, 8319. [CrossRef]
14. Cao, W.; Bu, J.; Zhao, C.; Wang, X.; Zhang, L.; Zhang, J. Stiffness Calculation for Negative Moment Region of Steel-Concrete Composite Beams considering the Influence of Cracking and Interface Slip. *Adv. Mater. Sci. Eng.* **2022**, *2022*, 1–12. [CrossRef]
15. Guo, Y.-T.; Yang, Y.; Song, S.-Y.; Fan, J.-S. Shear–slip failure in steel–concrete–steel composite beams with bidirectional webs. *Thin-Walled Struct.* **2021**, *164*, 107743. [CrossRef]
16. Dong, S.; Guo, J.; Zhang, C.; An, X.; Lu, M. Finite Element Analysis on Steel-Concrete Composite Beams Considering the Bond-Slip Effect on the Interface. *IOP Conf. Ser. Earth Environ. Sci.* **2021**, *719*, 022030. [CrossRef]
17. Tayeb, B.; Tahar, H.D. Improved analytical solution for slip and interfacial stress in composite steel-concrete beam bonded with an adhesive. *Adv. Mater. Res.* **2020**, *9*, 133–153.
18. Tan, H.; Qian, D.; Xu, Y.; Yuan, M.; Zhao, H. Analysis of Vertical Temperature Gradients and Their Effects on Hybrid Girder Cable-Stayed Bridges. *Sustainability* **2023**, *15*, 1053. [CrossRef]
19. Lu, H.; Zhang, C.; Jiao, L.; Wei, Y.; Zhang, Y. Analysis on the spatial-temporal evolution of urban agglomeration resilience: A case study in Chengdu-Chongqing Urban Agglomeration, China. *Int. J. Disaster Risk Reduct.* **2022**, *79*, 103167. [CrossRef]
20. *JTG/D61-01-2015*; Specification for Design and Construction of Highway Steel-Hybrid Composite Girder Bridges. People's Traffic Publishing House: Beijing, China, 2015.
21. Hao, Y. Study on Spatial Stress Analysis and Parameter Optimization of Construction Stage of Large Span V Braced Continuous Girder Bridge for High-Speed Railroad. Master's Thesis, Lanzhou Jiaotong University, Lanzhou, China, 2018.
22. Wang, J.Z.; Guo, J.F.; Mao, S.M. Study on the equivalent shear stiffness of shear nail groups considering interface slip. *World Bridges* **2019**, *47*, 43–47.
23. Zeng, Y.; Yu, H.; Tan, Y.; Tan, H.; Zheng, H. Dynamic Characteristics of a Double-Pylon Cable-Stayed Bridge with Steel Truss Girder and Single-Cable Plane. *Adv. Civ. Eng.* **2021**, *2021*, 9565730. [CrossRef]

24. Zeng, Y.; Zheng, H.; Jiang, Y.; Ran, J.; He, X. Modal Analysis of a Steel Truss Girder Cable-Stayed Bridge with Single Tower and Single Cable Plane. *Appl. Sci.* **2022**, *12*, 7627. [CrossRef]
25. Xin, J.; Jiang, Y.; Zhou, J.; Peng, L.; Liu, S.; Tang, Q. Bridge deformation prediction based on SHM data using improved VMD and conditional KDE. *Eng. Struct.* **2022**, *261*, 114285. [CrossRef]
26. Zeng, Y.; Qiu, Z.; Yang, C.; Su, H.; Xiang, Z.; Zhou, J. Fatigue experimental study on full-scale large sectional model of orthotropic steel deck of urban rail bridge. *Adv. Mech. Eng.* **2023**, *15*, 1–15. [CrossRef]

Disclaimer/Publisher's Note: The statements, opinions and data contained in all publications are solely those of the individual author(s) and contributor(s) and not of MDPI and/or the editor(s). MDPI and/or the editor(s) disclaim responsibility for any injury to people or property resulting from any ideas, methods, instructions or products referred to in the content.